Science and Technology of Advanced Materials

ISSN: 1468-6996 (Print) 1878-5514 (Online) Journal homepage: https://www.tandfonline.com/loi/tsta20

Parallel glide: flow of dislocations with internal stress source/sink distribution

Karlo T Raić

To cite this article: Karlo T Raić (2008) Parallel glide: flow of dislocations with internal stress source/sink distribution, Science and Technology of Advanced Materials, 9:1, 015008, DOI: 10.1088/1468-6996/9/1/015008

To link to this article: https://doi.org/10.1088/1468-6996/9/1/015008

IOP PUBLISHING SCIENCE AND TECHNOLOGY OF ADVANCED MATERIALS

Sci. Technol. Adv. Mater. **9** (2008) 015008 (7pp) doi:10.1088/1468-6996/9/1/015008

Parallel glide: flow of dislocations with internal stress source/sink distribution

Karlo T Raić

Faculty of Technology and Metallurgy, Belgrade University, Karnegijeva 4, POB 3503, 11120 Belgrade, Serbia

E-mail: karlo@tmf.bg.ac.yu

Received 19 September 2007
Accepted for publication 25 November 2007
Published 13 March 2008
Online at stacks.iop.org/STAM/9/015008

Abstract

The unexpected glide of dislocations on a plane parallel to the film/substrate interface in ultrathin copper films, which has been called *parallel glide* (Balk *et al* 2003 *Acta Metall*. **51** 447), is described using an analytical model. The phenomenon is observed as a problem involving inlet/outlet flow from different positions of a grain boundary into the grain channel. In this sense, parallel glide is presented as the flow of dislocations with an internal stress source/sink distribution.

Keywords: ultrathin films, dislocations, dynamics, metallic material

1. Introduction

It is well known that thin metal films exhibit mechanical properties very different from those of their bulk counterparts. Microstructural features that cause stresses in thin metal films exceed those of the corresponding bulk metal, in some cases by an order of magnitude [1, 2]. Unfortunately, this behavior is not yet completely understood. The remarkable model developed by Freund [3] and Nix [4] tried to describe the general trend of an increase in film strength with decreasing film thickness caused by threading dislocations. On the other hand, the constrained diffusional creep (CDC) model developed by Gao *et al* [5, 6], which describes the diffusive exchange of matter between the grain boundaries and the free surface of an unpassivated metal film rigidly attached to a substrate, has been employed to explain the thermal stress evolution in thin Cu films. Here, the concept of the flow of dislocations through the elemental grain cell with an internal stress source/sink distribution is presented in the context of the general laminar boundary layer strategy [7].

The plastic deformation and strengthening in metals can be related to a number of heterogeneous patterns, such as dislocation cells, slip bands, microshear bands, persistent slip bands and dislocation tangles, which are critical for obtaining good material properties. The main difficulty in modeling these patterns lies in the fact that the length scale of these phenomena is not large enough to treat them within the realm of a classical continuum mechanics framework. At the same time, the length scale is not small enough to observe these phenomena within the mechanics of a few dislocations, but rather through a thorough analysis of dislocation dynamics [8–10].

For this analysis, very important *in situ* transmission electron microscopy (TEM) studies focused on dislocations in thin metal films indicated the relevance of their motion during deformation [11] and their interaction with defects such as triple junctions, grain boundaries, and $\Sigma 3$ boundaries, as well as with film/substrate interfaces [12, 13]. Also, the prominent conclusion was that in the unpassivated Cu films, parallel glide dominated plasticity below a film thickness of approximately 400 nm. In this sense, both grain boundaries and triple junctions acted as sources for parallel glide dislocations [2].

2. Model formulation

2.1. Elemental cell—ideal grain channel

The thickness of advanced structural and thin-film materials are usually in the micron and submicron range. The geometrical constraints in these structures lead to fundamentally interesting effects of small-scale phenomena.

The experiment [2] analyzed in this model, which presented *in situ* TEM observations of thin copper films during thermal cycling, enables us to correlate these results with thermomechanical behavior, and explain the occurrence

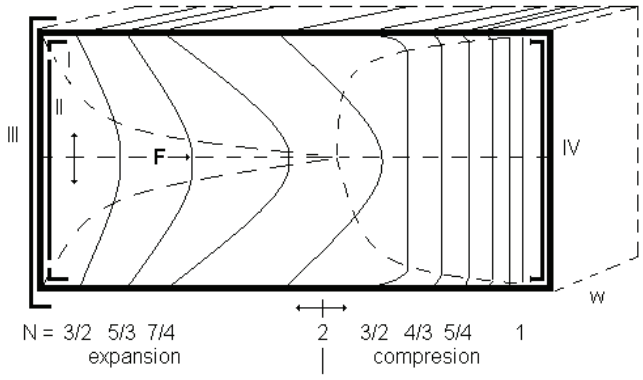

Figure 1. Schematic of elemental cell (ideal grain channel) with inlet/outlet region flow. I, II and III, possible positions of dislocation emission. IV, region of (compressed dislocations) reverse emission. w, width of the parallel plates.

of a unique form of dislocation-mediated plasticity. Given the fact that this new and unexpected dislocation mechanism involved the glide of dislocations parallel to the film/substrate interface, it is called *parallel glide*.

In a few words, the sequence of weak-beam TEM video images recorded during the cooling of a 200 nm Cu film was less than 26 min. A total of 10 dislocations were emitted sequentially from the source at the lower left triple junction. Dislocations were pushed forward by later dislocations, which in turn were not able to glide as far into the grain as the earlier ones. Accordingly, on the basis of the grain dimensions ($\approx$700 nm wide, $\approx 1\,\mu$m long) and the projected width of an inclined {111} plane of 70 nm, one can estimate the Reynolds number of dislocations gliding inside this 'rectangular duct' (see appendix).

Firstly, we can calculate the average velocity of dislocations $\bar{v} = 0.64\,\mathrm{nm\,s^{-1}}$. For this average velocity, the Reynolds number is $Re_{\mathrm{dis}} \approx 10^{-4} \ll 1$ (laminar regime—very slow motion).

However, the dislocations often travel 100 nm in a fraction of a second (steady-state flow sequence) and then remain immobile for several minutes before they move again ('jerky'/non-steady-state flow sequence). Now, the single dislocation velocity per total volume of the elemental cell is around $v_1 = 2500\,\mathrm{nm\,s^{-1}}$ or the Reynolds number is $Re = 0.4$ (laminar regime, $Re < 2300$). When the calculation is performed per unit volume of the sequence of the elemental cell, we have $Re_1 = 1620$. That is, during a single-dislocation motion, the assumption of laminar flow is also fulfilled.

Finally, the simple 'rectangular duct' (i.e. $70 \times 700 \times 1000\,\mathrm{nm}^3$) closed on the opposite side of the inlet will be the elemental cell or grain channel for dislocation gliding. A schematic of the elemental cell—ideal grain channel with inlet/outlet regions of dislocation flow with possible positions of dislocation emission (I, II and III) and a region of compressed dislocations or reverse emission (IV) is shown in figure 1. Note that this is a very simplified presentation of the model with only essential visual details.

2.2. Mathematical background

The deformation pattern generation, deformation-induced hardening and structurally induced hardening are complex phenomena involving nonlinear interaction among dislocations and the interaction of dislocations with interfaces. This further illuminates the fact that different deformation and strengthening mechanisms can explain similar phenomena. The length scale at which the deformation takes place, the mode of deformation and structure size are important factors that determine the corresponding dislocation mechanism [9, 10].

Consequently, in this paper, the nanoscale plasticity phenomena are based on newly developed discrete dislocation flow dynamics. The key concept is to use modeling approaches from laminar boundary layer theory to treat dislocation flow within the 'channel' provided by the thin film.

In many situations, the steady and/or unsteady laminar transport phenomena are described using partial differential equations. Usually, in such cases, we use the well-known techniques (method of combination of variables, method of separation of variables, method of sinusoidal response, integral methods, etc) that convert the problem of solving a partial differential equation into a problem of solving one or more ordinary differential equations (e.g. [14]). Here, we use a similar strategy but applied in a more general way.

Integral methods, based on setting balances for the control volume, are often used in practice for the cases of laminar boundary layers (e.g. [15]). The well-known problem in the application of these methods is the definition of satisfactory equations for the velocity distribution. According to the literature data, the use of a certain distribution equation is most commonly limited to the corresponding specific system. When the conditions are changed, it is necessary to choose a new, more appropriate distribution equation. To overcome this situation, an ordinary differential equation is proposed. Practically, the general equation of Navier–Stokes applied on laminar transport phenomena is simplified in two directions, namely, those along steady-state flow (Blasius equation) and non-steady-state flow/nonflow (Newton, Fourier and/or Fick's equations), and then substituted with an ordinary differential equation. Briefly, the similarity of solutions of these partial differential equations in analogous cases enables the substitution procedure through the following equation [7]:

$$f_1(N)\xi f_2(N) \pm \theta'' \pm f(m) = 0. \tag{1}$$

Introducing the relevant boundary conditions

- for steady-state-flow $\xi = y/\delta\chi$, when $\delta\chi = [2(N/M_\chi)(\mu\chi/\rho v^{\mathrm{dis}}_{\xi=1})]^{1/2}$
  $\xi = 0;\quad \mathrm{d}\theta/\mathrm{d}\xi = N;\quad \mathrm{d}^2\theta/\mathrm{d}\xi^2 = 0,$
  $\xi = 1;\quad \theta = 1;\quad \mathrm{d}\theta/\mathrm{d}\xi = 0,$
- for non-steady-state flow $\xi = y/\delta_\tau$ when $\delta_\tau = [2(N/M_\tau)(\mu\tau/\rho)]^{1/2}$
  $\xi = 0;\quad \mathrm{d}\Theta/\mathrm{d}\xi = N;\quad \mathrm{d}^2\Theta/\mathrm{d}\xi^2 = 0,$
  $\xi = 1;\quad \Theta = 1;\quad \mathrm{d}\Theta/\mathrm{d}\xi = 0.$
  the solution of equation (1) becomes the polynomial (see figure 2)

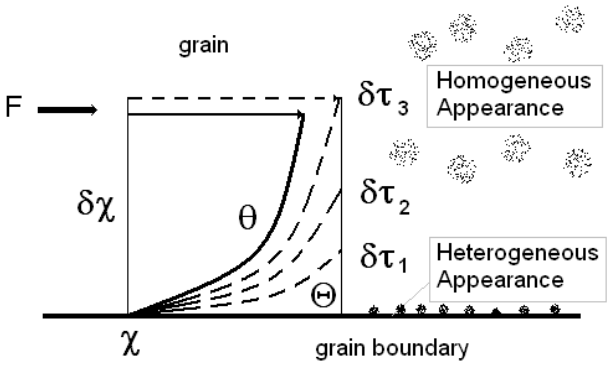

Figure 2. Description of steady and non-steady-state dislocation flow coupled in position χ.

- for steady-state-flow:

$$\theta = N\xi \pm 0.5\, f(m)\xi^2 \pm (N-1)\xi^{[N/\pm(N-1)]^{(\pm 1)^*}} \qquad (2a)$$

- for non-steady-state flow:

$$\Theta = 1 - \theta \qquad (2b)$$

where m is the characteristic whole number; M is the characteristic integral for position χ or time τ; $N = \mathrm{d}\theta/\mathrm{d}\xi|_{\xi=0} = -\mathrm{d}\Theta/\mathrm{d}\xi|_{\xi=0}$ is the dimensionless criterion; v_ξ^{dis} is the local velocity of a dislocation at the cross section; $v_{\xi=1}^{\mathrm{dis}}$ is the local core velocity of a dislocation at the position $\chi \sim x/(D_{\mathrm{e}}Re_{\mathrm{De}})$; $\delta\chi$ is the boundary layer thickness at position χ; $\xi = y/\delta\chi$ is the dimensionless distance from the interface at position χ; $\theta = v_\xi^{\mathrm{dis}}/v_{\xi=1}^{\mathrm{dis}}$ is the normalized dislocation distribution at position χ; $\theta''(\equiv -\Theta'') = \mathrm{d}^2\theta/\mathrm{d}\xi^2$ is the second-order derivative; $\Theta = (1-\theta)$ is the normalized distribution at time τ when $\xi = y/\delta_\tau$; δ_τ is the boundary layer thickness in the y-direction at time τ coupled with position χ.

For the solution of this equation, the normalized concentration distribution θ (or Θ) is considered in the most general sense of the term with an analogous meaning for the dislocation and/or force distributions as well as the internal stress source/sink distributions inside a grain channel.

In the first step of numerical treatment, the chosen instance will be the steady state flow of dislocations into the elemental cell—ideal grain channel with θ as the normalized dislocation distribution at some position χ.

The criterion $N = \mathrm{d}\theta/\mathrm{d}\xi|_{\xi=0}$ defines the state at the cross section perpendicular to the surface and for steady-state flow, enables the comparison and classification of laminar boundary layers within previously defined reference ($\theta_{N=1} = \xi$: simple Coutte flow) and boundary distributions (lower: $\theta_{N=0} = 1$: free flow; and upper: $\theta_{N=2} = 2\xi - \xi^2$: quadratic Poiseuille flow).

In other words, the solutions of equation (1) are families of polynomial curves grouped in regions [0;1/2], [1/2;1], [1;3/2] and [3/2;2] with appropriate signs '+' or '−' as well as N and $f(m)$ numbers. Consequently, these numbers are whole numbers or fractions (see table 1).

The functions $f_1(N)$ and $f2(N)$, for a certain region and chosen criterion N, also become constants in the form of a whole number or fraction. The core function $f(m) = \mathrm{d}\theta/\mathrm{d}\xi|_{\xi=1}$ indicates the homogeneous appearance coupled with variable core velocities $v_{\xi=1}^{\mathrm{dis}}$ at characteristic distance χ. On the other hand, the volume (continuous) homogeneity is incorporated into the basic distribution, through the correctly chosen region of criterion N change. The heterogeneous appearance along the grain boundary interfaces can be observed as a phenomenon in which obstacles change with the corresponding distribution θ in region [0;1/2]. Within borders resulting from laminar conditions, heterogeneous appearances are relatively independent. According to this concept, there exist two types of heterogeneous appearances: blade (b) and quasi-laminar (qL) with appropriate distributions and $\mathrm{FG_H}$ or N_{H} (see table 1 and figure 3). The effect of the obstacles on the dislocation distribution will be discussed elsewhere.

The 'simplified' equation (1) defines the Flux Gradient (FG) of the dislocations change phenomena

$$\mathrm{FG} = \int_0^1 \theta''\,\mathrm{d}\xi = \mathrm{d}\theta/\mathrm{d}\xi|_{\xi=0} + \mathrm{d}\theta/\mathrm{d}\xi|_{\xi=1} = N + f(m);$$
$$N \in [0,\,2], \qquad f(m) \in [0,\,\pm^\circ]. \qquad (3)$$

Note: when $[f(m) = 0] \Rightarrow \mathrm{FG} \equiv N$.

In principle, there are laminar layers with

- constant FG (or N) along the reference axis, i.e. the laminar boundary layer over a flat surface (example of nanosurface), and
- variable FG (or N), i.e. laminar entrance region flow, when every position of χ has its corresponding distribution (example of elemental cell or grain channel). These positions are changeable nodal locations and present the basic grids of the second steps of the numerical treatment.

A similar/analogous formulation is possible for non-steady-state situations.

The total coupling of the whole system is realized by the quantity m, which has a physical meaning of its own. Generally, m represents the ratio of formation to decomposition process parameter. In the case of the mobility of dislocations flowing through the grain channel, m is the ratio of internal stress sources to sinks.

The exact solution of starting partial differential equations (Blasius, Newton, Fourier or Fick's), the 'real' distribution (ϕ), has no error. The solution of proposed equation (1) has an approximate distribution (θ) in the form of polynomials with changeable coefficients and exponents. The difference ($\phi - \theta$) can be minimized, when necessary, by applying the numerical procedure that takes into account the continuous correction of the diffusivity in accordance with the actual distribution in the laminar boundary layer, i.e. the fully implicit or modified explicit finite difference method.

2.3. Plasticity of ultrathin films

The model is designed to simulate the dynamics of dislocations in (χ, ξ) dimensions under an applied stress, σ.

Table 1. Elements of steady-state dislocation flow model.

Ordinary differential equation:	$f_1(N)\xi^{f_2(N)} \pm \theta'' \pm f(m) = 0$
General solution: when $f(m) = 0$	$\theta = N\xi \pm 0.5\,f(m)\xi^2 \pm (N-1)\xi^{[N/\pm(N-1)]^{(\pm1)^*}}$
Reference distribution:	$\theta_{N=1} = \xi$: simple Coutte flow
Boundary distributions:	
Lower:	$\theta_{N=0} = 1$: free flow
Upper:	$\theta_{N=2} = 2\xi - \xi^2$: quadratic Poiseuille flow

Regions	[0; 1/2]	[1/2; 1]	[1; 3/2]	[3/2; 2]
N	$1 - m/(m+1)$	$m/(m+1)$	$2 - m/(m+1)$	$1 + m/(m+1)$
$f(m)$	$2 - 1/m$	$2 - m$	m	$1/m$
$[N/\pm(N-1)]^{(\pm1)}$	$[-(N-1)/N]\,qL^*$	$[N/-(N-1)]$	$[N/(N-1)]$	$[N/(N-1)]$
$(N-1)\xi^{[N/\pm(N-1)](\pm1)^*}$	$0\,[f(m) = 0]\,b^*$			
B.C.	$\xi = 0 \Rightarrow \theta = 0$	$\xi = 0 \Rightarrow \theta = 0$	$\xi = 0 \Rightarrow \theta = 0$	$\xi = 0 \Rightarrow \theta = 0$
when $f(m) = 0$:	$\xi = 1 \Rightarrow \theta = 1$ ($\xi = 1 \Rightarrow \theta \neq 1\,b^*$)	$\xi = 1 \Rightarrow \theta = 1$	$\xi = 1 \Rightarrow \theta = 1$	$\xi = 1 \Rightarrow \theta = 1$
when $f(m) \neq 0$:	$\xi = 1 \Rightarrow \theta \neq 1$	$\xi = 1 \Rightarrow \theta \neq 1$	$\xi = 1 \Rightarrow \theta \neq 1$	$\xi = 1 \Rightarrow \theta \neq 1$
Example for $m = 2;\ f(m) = 0$	$1/3\xi + 2/3\xi^2\,qL^*$ $1/3\xi\,b^*$	$2/3\xi + 1/3\xi^2$	$4/3\xi - 1/3\xi^4$	$5/3\xi - 2/3\xi^{5/2}$
$\mathrm{d}\theta/\mathrm{d}\xi\|_{\xi=0}$ (e.g. for $m = 2$; $f(m) = 0$)	N (e.g. 1/3) qL^* N (e.g. 1/3) b^*	N (e.g. 2/3)	N (e.g. 4/3)	N (e.g. 5/3)
$\mathrm{d}\theta/\mathrm{d}\xi\|_{\xi=1,\,f(m)=0}$	$\neq 0$	$\neq 0$	0	0
$\mathrm{d}\theta/\mathrm{d}\xi\|_{\xi=1,\,f(m)\neq0}$	$\neq 0$	$\neq 0$	$\neq 0$	$\neq 0$
FG – code	$\mathrm{D}\theta/\mathrm{d}\xi\|_{\xi=0}$ $N\,qL^*$ $N\,b^*$	${}_1\int^0 \theta''\mathrm{d}\xi$	${}_1\int^0 \theta''\mathrm{d}\xi$	${}_1\int^0 \theta''\mathrm{d}\xi$

qL^*: quasi-Laminar; b^*: 'blade'.

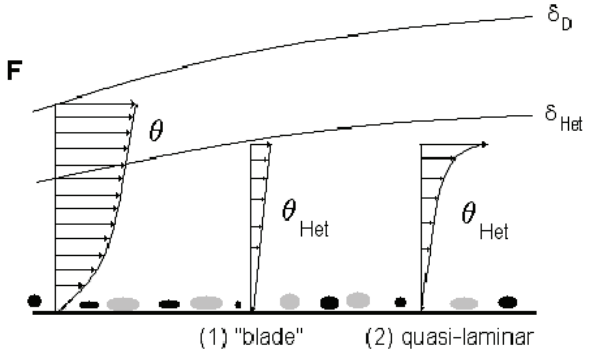

Figure 3. Heterogeneous appearances: blade (b) and quasi-laminar (qL) with appropriate distributions (δ_{D}, boundary for dislocation distribution θ; δ_{Het}, boundary for heterogeneous appearance θ_{Het}).

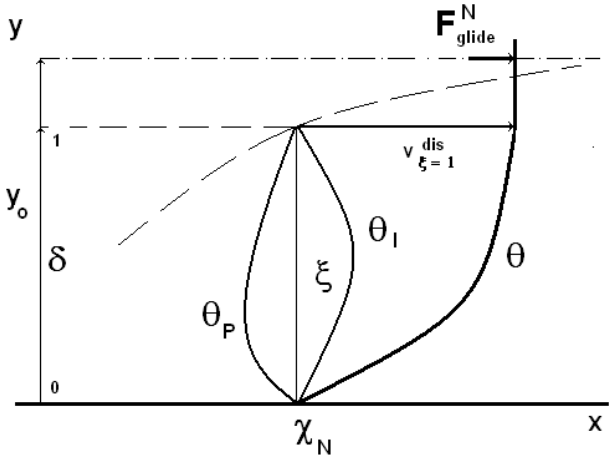

Figure 4. Dislocation at position χ_N presented by polynomial θ coupled by force F^N_{glide} with corresponding distributions of the internal stress source $\theta_I = \theta - \theta_{N=1}$ and sink $\theta_P = \theta_{N=2} - \theta$.

To define the stress fields of arbitrarily curved dislocations, these are approximated by the polynomials given by equation (2) (table 1). To establish the dislocation dynamics, the force on every polynomial position must be defined (figure 4). Only dislocation glide is considered.

For a general stress state σ, the force per unit length on a dislocation with Burger vector b and line element s is given by

$$F^N_{\mathrm{glide}} = (\sigma \cdot \mathrm{b}) \times \mathrm{s}. \tag{4}$$

Equation (4), known as the Peach–Koehler equation, provides the fundamental relation between the macroscopic stress and strain and the microscopic mechanisms of the formation.

The stress σ is composed of the internal stresses, caused by the other dislocations and the dislocation line itself, the

external stresses resulting from the load, and the stresses needed to realize the boundary conditions. To compute the internal stress at position χ, the stress contributions from all segments of the same dislocation and of all other dislocations can be added by correctly choosing criterion N.

Once the forces are defined, the polynomials/dislocations are moved according to a viscous drag law

$$v^{\mathrm{dis}}_{\xi=1} = F^{N}_{\mathrm{glide}}/B. \tag{5}$$

Note: $F^{N}_{\mathrm{glide}} = f^{\mathrm{dis}}_{\xi=1}$ for any χ and $F^{0} = f^{\mathrm{dis}}_{\xi=1}$ when $\chi = 0$ or simply $F^{N}_{\mathrm{glide}} = f(\chi)$.

Generally, one can express the local velocity of a dislocation at the cross section ξ as

$$v^{\mathrm{dis}}_{\xi} = f^{\mathrm{dis}}_{\xi}/B, \tag{6}$$

where f^{dis}_{ξ} is the related dislocation force.

Finally, one can obtain the normalized dislocation distribution at position χ as

$$\theta = v^{\mathrm{dis}}_{\xi}/v^{\mathrm{dis}}_{\xi=1} = f^{\mathrm{dis}}_{\xi}/f^{\mathrm{dis}}_{\xi=1} = f^{\mathrm{dis}}_{\xi}/F^{N}_{\mathrm{glide}}$$

where B is the drag coefficient, i.e. $B = 1.7 \times 10^{-5}$ Pa s for copper [16].

In this concept, a single dislocation is traveling from one side of a grain to another, passing characteristic positions χ with well-determined internal stresses. In fact, the internal stress at position χ is defined by the internal stress source θ_I/sink θ_P distribution.

3. Dislocation flow with internal stress source/sink distribution

The elemental cell (ideal grain channel) has the inlet region with dislocation emission (with N criterions in the range $\in [3/2; 2]$) and closed outlet region with dislocations compression/reverse emission (with N criterions in the range $\in [1; 3/2]$). Other combinations of N criterion ranges are also possible. For the simplest case, the core function that indicates the homogeneous appearance coupled with variable core velocities $v^{\mathrm{dis}}_{\xi=1}$ at characteristic distances along the interface is $f(m) = \mathrm{d}\theta/\mathrm{d}\xi|_{\xi=1} \approx 0$; thus, FG $\equiv N$.

3.1. Emission (region N ∈[3/2;2])

The dynamics of dislocation flow in the entrance section of the grain channel depends on disturbances created before or at the entrance. Such disturbances in the dislocation flow are dissipated as the dislocations flow through the grain channel. When dislocations start to enter the grain channel the boundary layer begins forming at the entrance. The dislocation profile becomes fully developed after the edge of the boundary layer coincides with the axis of the grain channel. The dislocation-dynamics conditions at the entrance of the grain channel greatly affect the length required for the fully developed dislocation profile to form. The entrance to the grain channel involves either a sudden expansion or contraction in the cross-sectional area of dislocation flow, and for this reason, the configuration of the entrance is an important factor in studying the dislocations flow downstream.

According to this concept, in the formation of a laminar boundary layer, instead of only an external stress source, there is also an internal one that ensures the necessary flux for the basic flow of the dislocations and forms its own stress source field. At the same time, an internal stress sink appears as a measure of dislocation flow resistance. In the case of a freely formed boundary layer, the internal source and sink are set to be equal so that the internal stress difference is zero. For the case of a transitional boundary layer appearing during flow between two parallel plates, a stress difference appears, which affects the ratio of the internal source to the internal sink. The internal sink decreases until the boundary layer is formed. In the case of the formed boundary layer, the total internal source is established along the whole cross section (there is no sink). In the literature, this case is known as Poiseulle flow with characteristic criterion $N = 2$. Thus, the transitional boundary layer tends to the boundary case $N = 2$. The internal stress source and sink are reflected in the dislocation distribution. The corresponding distribution of the internal stress source is

$$\theta_I = \theta - \theta_{N=1},$$

and of the stress sink is

$$\theta_P = \theta_{N=2} - \theta,$$

where $\theta_{I,P} = f^{I,P}_{\xi}/f^{I,P}_{\xi=1}$ is the normalized distribution of stress source (I) or sink (P) at position χ with the following boundary conditions.

$$\begin{aligned} &\xi = 0; && \mathrm{d}\theta_I/\mathrm{d}\xi = N - 1, \\ &\xi = 0; && \mathrm{d}\theta_P/\mathrm{d}\xi = 2 - N, \\ &\xi = 1; && \theta_{I,P} = 0. \end{aligned}$$

Forces $f^{I}_{\xi=1}$ and $f^{P}_{\xi=1}$ are related to F^{N}_{glide} as $f^{I}_{\xi=1} = -f^{P}_{\xi=1} = f(F^{N}_{\mathrm{glide}})$.

If the appropriate criteria I and P are $I = \mathrm{d}\theta_I/\mathrm{d}\xi|_{\xi=0}$ and $P = \mathrm{d}\theta_P/\mathrm{d}\xi|_{\xi=0}$, then the first derivates for $\xi = 0$ yield

$$N = 1 + I\,(= 2 - P) \text{ or } I + P = 1.$$

This furthermore enables an estimation of criterion N as

$$N = 1 + [m/(m+1)], \qquad m = I/P = 1, 2, 3, 4, \ldots, \infty.$$

Thus, the values of criterion N for the inlet region of the elemental cell lie between 3/2 and 2 (figure 5).

On the basis of the expression $m = I/P$ and the estimation of m at the beginning ($m = 1$) and end ($m = \infty$) of the zone of forming a boundary layer, it is concluded that the following analogy holds:

$$I \to y_0, \qquad P \to (y_0 - \delta_\chi); \qquad \text{i.e. } m \approx y_0/(y_0 - \delta_\chi),$$

where, y_0 is half the distance between parallel plates.

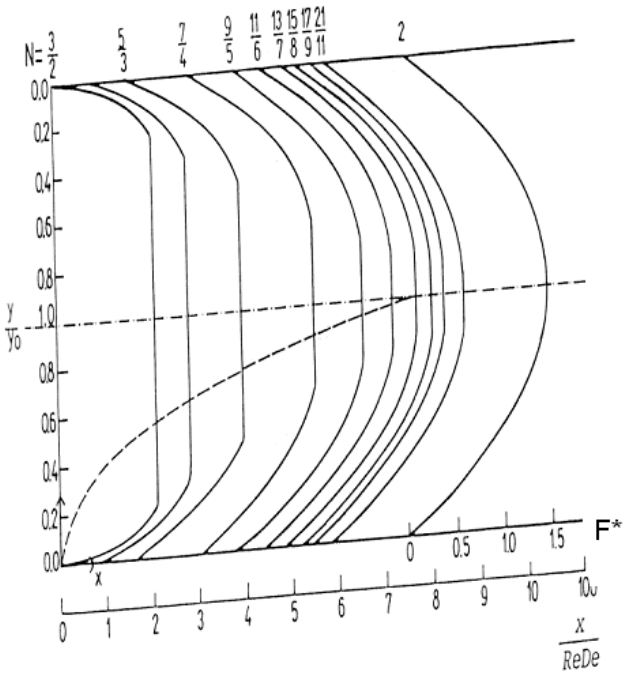

Figure 5. Dislocation distribution with values of the N criterion at certain cross sections in the zone in which a boundary layer is formed, i.e. region of expansion.

On the basis of these simple relations, one obtains for the dimensionless distance ratio

$$\delta^* = \delta\chi/y_0 = (2N-3)/(N-1), \tag{7}$$

and for the dimensionless ratio of the forces in the flow axis

$$F^* = \frac{F^N_{\text{glide}}}{F^0_{\text{glide}}} = \left[1 - \frac{N(2N-3)}{2(2N-1)(N-1)}\right]^{-1}. \tag{8}$$

The dependence of these quantities (δ^*, F^*) on a third dimensionless parameter $\chi = x/(D_e Re_{De})$ is determined by balancing the control volume, for example, $Re_{De} = 0.4$ and $D_e = 127$ nm (see figure 5).

The theoretical variation of the force F^N_{glide} at the edge of the boundary layer as a function of the distance from the entrance of the elemental cell or grain channel is presented in figure 6.

The every position χ has its corresponding distribution. These positions are changeable nodal locations and present the basic grids of the second steps of the numerical treatment.

3.2. Compression—reverse emission (region N ∈[3/2;2])

After the critical distance at which point Poiseulle flow is established, dislocations start to compress each other because there is no place for further development. The corresponding distribution of the internal stress source is

$$\theta_I = \theta_{N=2} - \theta,$$

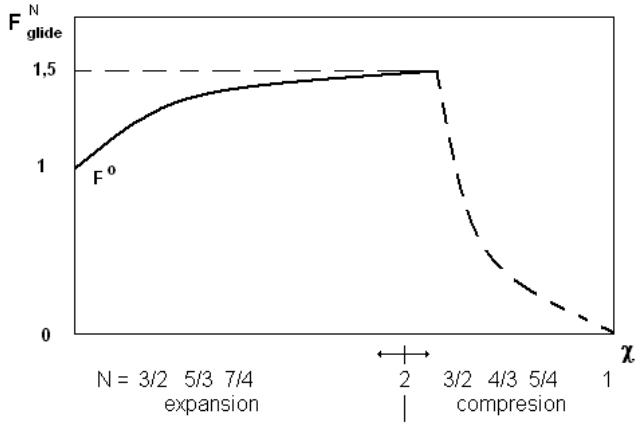

Figure 6. Variation of force F^N_{glide} at edge of boundary layer as a function of distance χ from the entrance of the elemental cell—grain channel.

and that of the stress sink is

$$\theta_P = \theta_{N-1} + \theta.$$

Accordingly, the first derivatives for $\xi = 0$ yield $N = 2 - I\,(= 1 + P)$ or $I + P = 1$.

This enables the estimation of criterion N, but now as $N = 2 - [m/(m+1)]$, where $m = I/P = 1, 2, 3, 4, \ldots, \infty$. Thus, the values of criterion N for the established inverse laminar boundary layer lie between 3/2 and 1 (figure 1).

Similarly, the following analogy holds:

$$I \to (y_0 - \delta_\chi); \qquad P \to y_0; \qquad \text{i.e. } m \approx (y_0 - \delta_\chi)/y_0.$$

On the basis of these simple relations, one can obtain

$$\delta^* = \delta\chi/y_0 = f_1(N) \text{ and } F^* = F^N_{\text{glide}}/F^0_{\text{glide}} = f_2(N).$$

Now, the dislocation velocity in the potential flow of the cross section at position χ, because of enormous compression, becomes zero, i.e. $F^N_{\text{glide}} \to 0$ (see figure 6).

4. Conclusion

In this study, we dealt with a theoretical analysis of parallel dislocation glide in thin metal films using a laminar boundary layer approach of the Navier–Stokes type. The physical relationship between the discrete problem and the continuum description was presented via the Peach–Koehler equation.

The parallel glide of dislocations, as a discrete nanoscopic phenomenon, was observed as an inlet/outlet region flow problem that occurred from different positions of the grain boundary into the grain and described as the flow of dislocations with an internal stress source/sink distribution.

The presented concept is imagined as a flexible iterative system for the following experimental data. It is shown in the simplified form for the sake of clarity. Only the essential instructions of simulation procedure are given. To solve the real situation, it is necessary to determine the following: (i) the interval/range of N criterion change,

(ii) the deformation of the dislocation velocity distribution in the direction perpendicular to the parallel surfaces caused by the heterogeneous appearances and (iii) the action of the $f(m)$ or homogeneous appearances.

The concept may provide a useful viewpoint that contrasts with/complements other theories such as phase-field or level-set methods that are concurrently being developed for dislocations.

Finally, a comprehensive understanding of the link between dislocation motion and the thermomechanical behavior of unpassivated thin films does not yet exist, and the need for careful TEM studies remains. In this sense, the aim of this study is to shed a different light in the explanation on the interaction between gliding dislocations and the grain surrounding.

Appendix

(a)

- Volume of the elemental cell—ideal grain channel, $V = 70 \times 700 \times 1000 = 49 \times 10^6\,\mathrm{nm}^3$
- Average velocity of dislocations, $\bar{v} = 1000\,\mathrm{nm}/26 \times 60\,\mathrm{s} = 0.64\,\mathrm{nm\,s}^{-1}$
- Density of dislocations, $\rho = 10$ dislocations$/V = 0.2 \times 10^{-6}\,\mathrm{dis\,nm}^{-3}$
- Dislocations viscosity, $\mu = (10$ dislocations$\mathrm{A}^{-1})/(Y/\bar{v}) = 0.156\,\mathrm{dis\,s\,nm}^{-2}$
- $A = 1000 \times 70 = 7 \times 10^4\,\mathrm{nm}^2$, $Y = 700\,\mathrm{nm}$
- Equivalent diameter of the elemental cell—ideal grain channel,
- $D_\mathrm{e} = 4$ (dislocation flow area)/('wetted perimeter')$= 4(70 \times 700)/(2 \times 70 + 2 \times 700) = 127\,\mathrm{nm}$
- Reynolds number for average velocity of dislocations, $Re_\mathrm{dis} = \bar{v} D_\mathrm{e} \rho/\mu \approx 10^{-4} \ll 1$ (laminar regime—very slow motion).

(b)

- Velocity of the single-dislocation sequence motion, $v_1 = 100\,\mathrm{nm}/0.04\,\mathrm{s} = 2500\,\mathrm{nm\,s}^{-1}$
- (Note that video frames were recorded at 25 frames s^{-1}, thus, $1/25 = 0.04\,\mathrm{s}$)
- Reynolds number for the velocity of the single-dislocation sequence motion for total volume of the elemental cell, $Re_\mathrm{dis1} = v_1 D_\mathrm{e} \rho/\mu = 0,4$ (laminar regime, $Re < 2300$).

(c)

- Volume of the sequence of the elemental cell, $V_1 = 70 \times 700 \times 100 = 49 \times 10^5\,\mathrm{nm}^3$
- Density of a dislocation, $\rho_1 = 1$ dislocation$/V_1 = 0.2 \times 10^{-6}\,\mathrm{dis\,nm}^{-3}$
- Dislocation viscosity, $\mu_1 = (1$ dislocation $\mathrm{A}^{-1})/(Y/v_1) = 4 \times 10^{-5}\,\mathrm{dis\,s\,nm}^{-2}$
- $A = 100 \times 70 = 7 \times 10^3\,\mathrm{nm}^2$, $Y = 700\,\mathrm{nm}$
- Reynolds number for the velocity of the single-dislocation sequence motion in the sequence of the elemental cell, $Re_1 = v_1 D_\mathrm{e} \rho_1/\mu_1 = 1620$ (laminar regime, $Re < 2300$).

References

[1] Arzt E 1998 *Acta Mater.* **46** 5611
[2] Balk T J, Dehm G and Arzt E 2003 *Acta Metall.* **51** 4471
[3] Freund L B 1987 *J. Appl. Mech.* **54** 553
[4] Nix W D 1989 *Metall. Trans.* A **20** 2217
[5] Gao H, Zhang L, Nix W D, Thompson C V and Arzt E 1999 *Acta Mater.* **47** 2865
[6] Gao H, Huang Y, Nix W D and Hutchinson J W 1999 *J. Mech. Phys. Solids* **47** 1239
[7] Raic K T 2000 *Interface Sci.* **8** 85
[8] Shafique M A, Khana S M A, Zbib H M and Hughes D A 2004 *Int. J. Plasticity* **20** 1059
[9] Zbib H M and Diaz de la Rubia T 2002 *Int. J. Plasticity* **18** 1133
[10] Zbib H M and Khraishi T A 2005 Dislocation dynamics *Handbook of Materials Modeling* ed S Yip (Berlin: Springer) 1097
[11] Kobrinsky M J, Dehm G, Thompson C V and Arzt E 2001 *Acta Mater.* **49** 3597
[12] Balk T J, Dehm G and Arzt E 2001 *Dislocations and Deformation Mechanisms in Thin Films and Small Structures* (*Materials Research Society Symposia Proceedings* vol 673) ed O Kraft, K W Schwarz, S P Baker, L B Freund and R Hull (Warrendale, PA: Material Research Society) p P2.7.1
[13] Balk T J, Dehm G and Arzt E 2002 *Thin Films—Stresses and Mechanical Properties* (*Materials Research Society Symposia Proceedings* vol 695) ed C S Ozkan, R C Cammarata, L B Frund and H Gao (Warrendale, PA: Material Research Society) p L2.7.1
[14] Bird R B, Stewart W E and Lightfoot E D 2002 *Transport Phenomena* 2nd edn (New York: Wiley)
[15] Schlichting H and Gersten K 2000 *Boundary-Layer Theory* 8th edn (Berlin: Springer)
[16] Jassby K and Vreeland Jr T 1970 *Phil. Mag.* A **21** 1147